

Quantitative cerebrovascular pathology in a community-based cohort of older adults



Swati Rane^{a,*}, Natalie Koh^a, Peter Boord^a, Tara Madhyastha^a, Mary K. Askren^a, Suman Jayadev^a, Brenna Cholerton^b, Eric Larson^c, Thomas J. Grabowski^a

^a Radiology, University of Washington Medical Center, Seattle, WA, USA

^b Department of Pathology, Stanford University School of Medicine, Palo Alto, CA, USA

^c Group Health Research Institute, Seattle, WA, USA

ARTICLE INFO

Article history:

Received 28 July 2017

Received in revised form 8 January 2018

Accepted 9 January 2018

Available online 31 January 2018

Keywords:

Aging

Cerebral blood flow

Cerebrovascular disease

ASL

White matter disease

BOLD contrast

CVR

ABSTRACT

Cerebrovascular disease, especially small vessel pathology, is the leading comorbidity in degenerative disorders. We applied arterial spin labeling and cerebrovascular reserve (CVR) imaging to quantify small vessel disease and study its effect on cognitive symptoms in nondemented older adults from a community-based cohort. We evaluated baseline cerebral blood flow (CBF) using arterial spin labeling and percent signal change as a marker of CVR using blood-oxygen level-dependent imaging following a breath-hold stimulus. Measurements were performed in and near white matter hyperintensities, which are currently the standard to assess severity of vascular pathology. We show that similar to other studies (1) CBF and CVR are markedly reduced in the hyperintensities as well as in the tissue surrounding them, indicating susceptibility to infarction; (2) low CBF and CVR are significantly correlated with poor cognitive performance; and (3) in addition, compared to a 58.4% reduction in CBF, larger exhaustion (79.3%) of CVR was observed in the hyperintensities with a faster, nonlinear rate of decline. We conclude that CVR may be a more sensitive biomarker of small vessel disease than CBF.

© 2018 Elsevier Inc. All rights reserved.

1. Introduction

Small vessel cerebrovascular disease is a common occurrence in aging and related disorders such as Alzheimer's disease (AD) (Al-Bachari et al., 2014; Pantoni, 2010; Wardlaw et al., 2013). It is a major contributor to mixed dementia pathology and has similar risk factors as those for cognitive decline (White et al., 1996). Typical cerebrovascular pathology associated with dementia consists of cortical and subcortical infarcts, microbleeds, increased perivascular spaces, reduced perfusion, and tissue atrophy (Bots et al., 1997; Esiri et al., 1999). Histopathological studies show that individuals with AD show increased basal membrane thickening, collagenous deposits, and damaged pericytes in the microvasculature compared to age-matched older adults (Farkas and Luiten, 2001). The resulting vascular insufficiency causes neuronal damage and, subsequently, cognitive decline, which progresses slowly. Therefore, sensitive methods are needed to monitor the

advancing vascular pathology to subsequently arrest disease progression.

Recent advances in neuroimaging have provided tremendous insights into small vessel disease, especially by distinguishing normal-appearing brain matter from pathological tissue. One important imaging measure is the volume of white matter hyperintensities (WMHs), that is, regions of brain tissue, which appear bright on a T2-weighted magnetic resonance imaging (MRI) scan, in deep white matter tissue (Au et al., 2006; Prins and Scheltens, 2015; de Groot et al., 2000). WMHs are thought to occur because of chronic hypoperfusion as a result of the small vessel disease. A higher volume of WMHs is associated with poorer cognitive outcome in older adults (Bahrani et al., 2017; Brickman et al., 2009; van Dalen et al., 2016; Prins and Scheltens, 2015). It is also associated with poor executive function, especially processing speed for executive tasks (Au et al., 2006; Smith et al., 2011). Although antihypertensive treatments manage to slow their development (Dufouil et al., 2005; Liao et al., 1996), these hyperintensities likely represent tissue that is damaged and is currently unresponsive to vascular therapies.

Cerebral blood flow (CBF) imaging is another imaging marker that can detect ischemic tissue (Detre et al., 1994; Wong et al., 1999). Similarly, cerebrovascular reserve (CVR) mapping using

* Corresponding author at: Radiology, University of Washington Medical Center, 1959 Pacific St. NE, Seattle, WA 98195, USA. Tel.: +1 206 543 6195; fax: +1 404 202 7338.

E-mail address: srleven@uw.edu (S. Rane).

Table 1
Demographic information (n = 28) and summary statistics

Description	Mean	Standard deviation
Age (years)	76.4	7.1
Gender	13 M/15 F	
APOE-ε4 carriers	5	
Mean arterial pressure (mm Hg)	91	11
Heart rate (bpm)	65	9
MMSE	28	1
Trails A	30	11
Trails B	80	31
Logical memory	15	3
White matter hyperintensities (% of total ICV) ^a	0.21	0.21

Key: APOE, apolipoprotein E; ICV, intracranial volume; MMSE, Mini-Mental State Examination.

^a White matter hyperintensities burden range: 0.01–0.8, includes both periventricular and deep white matter hyperintensities.

hypercapnia induced by acetazolamide, breath-hold, or manipulating inhaled gas can identify tissue with low or exhausted vascular reserve (Bright and Murphy, 2013; Gückel et al., 1996; Kastrup et al., 1998). Reduced CBF reflects presence of primary vasculopathy such as atherosclerosis of large vessels, microvascular injury (basal membrane thickening, pericytic degeneration, and collagen deposits, mentioned earlier), or a reduced metabolic demand due to neuronal dysfunction/loss (Farkas and Luiten, 2001). A reduced CVR may indicate either microvascular injury or an exhausted reserve. We believe that a combinatorial approach may provide better understanding of the underlying vascular physiology. One study shows that CBF is reduced in the tissue surrounding the WMHs and does indeed indicate tissue at risk of infarction as seen on a longitudinal scan 2 years later (Promjunyakul et al., 2015). In general, WMHs have been extensively studied using CBF.

However, CVR measurements in WMHs and direct comparisons of sensitivity of CBF and CVR to detect progression of small vessel disease are limited with variable results. Sam et al. (2016) measured white matter (WM) integrity, T2, and CBF in WMHs and normal-appearing WM and found that reductions in CVR preceded hyperintensity development in normal WM. Another contrast-based study showed reduced baseline CBF and blood volume as well as reduced changes in CBF and blood volume in WMHs during an acetazolamide challenge, compared to normal-appearing WM (Marstrand et al., 2002). The cerebral autosomal dominant arteriopathy with subcortical infarcts and leukoencephalopathy study measured similar baseline CBF and CVR (with acetazolamide) and reduced CVR (not CBF) in WMHs (Liem et al., 2009). Reduced CBF and CVR in the WMHs, compared to normal-appearing WM, have been reported in a wide variety of diseases such as type 2 diabetes (Novak et al., 2006), small vessel disease (Molina et al., 1999), and AD (Makedonov et al., 2013). In this study, we compare CBF and CVR to assess which biomarker is more sensitive to small vessel disease pathology and cognitive function in a community-based cohort of older adults.

Specifically, we explore CBF and CVR measurements as markers of ischemic tissue in and around the WMHs. We believe that these markers have the potential to detect normal-appearing tissue that is susceptible to ischemic events and which has a high risk of developing into hyperintensities. We hypothesize that, similar to CBF, CVR will also be reduced in the regions of the WMHs. It will also be lower in the tissue surrounding the hyperintensities. We used arterial spin labeling (ASL) to measure CBF and breath-hold blood-oxygen level-dependent (BOLD) imaging to measure CVR in a community-based cohort of older adults (Bright and Murphy, 2013; Detre et al., 1994). We performed comparisons of CBF and CVR in gray matter (GM), normal-appearing WM, and the hyperintensity regions. Correlation

with overall cognitive and executive function was also assessed. The advantage of this study is that we applied a noninvasive approach to measure CBF and CVR. Furthermore, we used a simple breath-hold paradigm, which does not require any specialized equipment.

2. Material and methods

Thirty older adults (76.4 ± 7.1 years, 13 M/15 F) were recruited from the community-based Adult Changes in Thought cohort (ACT; Montine et al., 2012). ACT is a population-based study of dementia risk designed to prospectively examine the incidence of AD and dementia, as well as risk factors of these diseases, in a cohort representative of the Group Health Cooperative in Seattle. Nondemented subjects, who are cognitively normal or mildly cognitively impaired with no effect on daily living, are included in this cohort. All participants provided written informed consent to participate in the present study, which was conducted according to the Declaration of Helsinki and subsequent revisions. The study was approved by the Institutional Review Board at University of Washington, Seattle. Demographic data are shown in Table 1. All subjects underwent the National Alzheimer Coordinating Center Uniform Data Set cognitive battery including Trails A, Trails B, Mini-Mental State Examination (MMSE), and logical memory (Beekly et al., 2007; Folstein et al., 1975; Mack et al., 1992; Tombaugh, 2004; Wechsler, 1945, 2014). Cognitive diagnosis was adjudicated during a clinical case consensus diagnosis conference consisting of neurologists, psychiatrists, neuropsychologists, and other study clinicians. These subjects underwent both a pseudo-continuous ASL (pCASL) scan to measure CBF and a breath-hold BOLD MRI for measuring CVR on a Philips 3T Achieva scanner with a 32-channel SENSEitivity Encoding (SENSE) coil reception. Of these, 2 subjects had low MMSE scores (20 and 22) and hence were excluded from this study.

2.1. Imaging

Each session included a structural T1-weighted image using a 3D-turbo field echo acquisition with TR/TE = 9.2/3.5 ms, resolution = $1 \times 1 \times 1$ mm³ for image registration and segmentation purposes. Fluid Attenuated Inversion Recovery (FLAIR) images were acquired to detect WMHs with the following parameters: repetition time (TR)/inversion time (TI)/echo time (TE) = 5000/1800/293 ms, resolution = $1 \times 1 \times 1$ mm³. Pseudo-continuous ASL imaging parameters were TR/TE = 5000/35 ms, 30 pairs of control and label images, resolution = $3.5 \times 3.5 \times 5$ mm³, background suppression (BS1 = 1710 ms and BS2 = 2860 ms), label plane 80 mm below the center of the imaging volume, labeling duration, τ = 1650 ms, post-labeling delay, ω = 2000 ms, total acquisition time = 5 minutes. For the 6-minute breath-hold BOLD MRI implementation, subjects were trained outside the scanner to perform 6 paced breaths followed by a breath-hold for 10–15 seconds (as feasible for the subject) and then by free breathing. The breath-hold was initiated at the end of an exhale (Bright and Murphy, 2013). Blocks of paced breathing, breath-hold, and free breathing were repeated for a total of 6 times. Other imaging parameters were resolution = $3.5 \times 3.5 \times 3.5$ mm³, TR/TE = 2500/35 ms, dynamics = 122, and SENSE factor = 2. The same stimulus paradigm was repeated inside the scanner. The breathing pattern of the subject was recorded using respiratory bellows and used as the time course for analyses. The time course was also used to determine if subjects followed the breathing instructions inside the scanner.

2.2. Analyses

In order to quantify CBF, the pCASL perfusion weighted images were motion corrected and registered to the first dynamic image

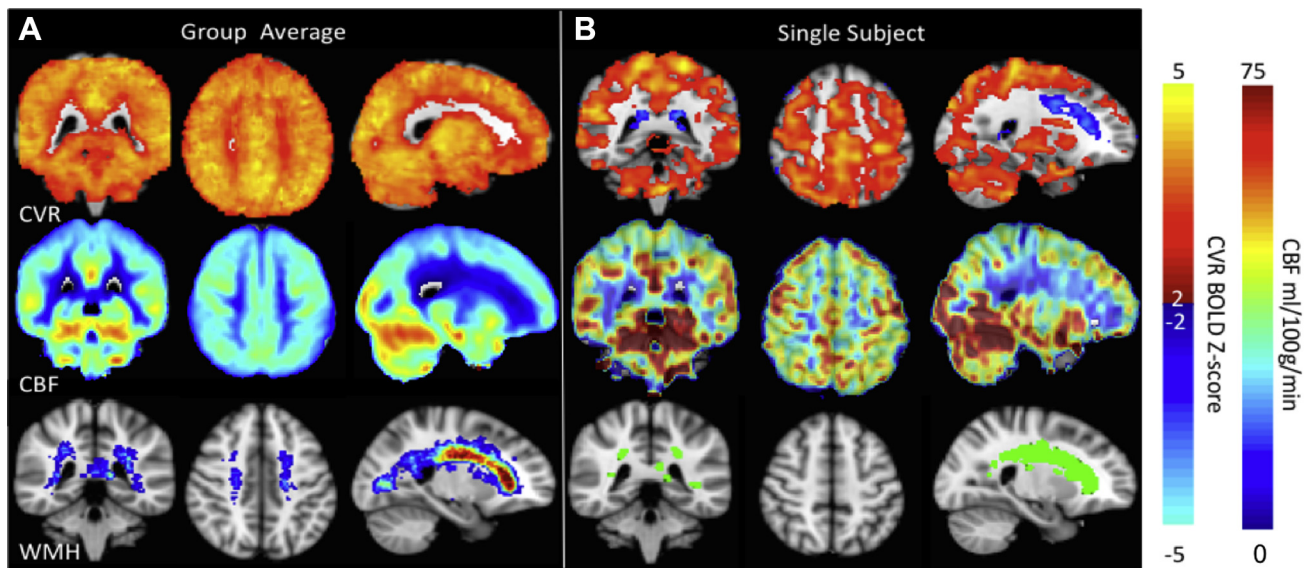


Fig. 1. Group-level (A) and single-subject (B) maps of percent BOLD signal change (cerebrovascular reserve, CVR) during a breath-hold paradigm (top row), cerebral blood flow i.e., CBF (middle row), and frequency of WMHs (bottom row). CVR maps represent the magnitude of the dilatatory response of the cerebral vasculature to a breath-hold. The group white matter map is a map of frequency of the occurrences of WMHs. Red voxels indicate a higher frequency; more subjects had WMHs in those voxel locations, and blue indicates a lower frequency; fewer subjects had infarcted white matter in the corresponding voxel locations. The green mask represents WMH segmentation in a single subject in Fig. 1B. The single-subject CVR map shows negative BOLD signal near the WMHs, likely, due to steal phenomenon or due to a combined effect of partial voluming and CSF fluid movement in ventricles during breath-hold. Abbreviations: BOLD, blood-oxygen level-dependent; CBF, cerebral blood flow; CVR, cerebrovascular reserve; WMH, white matter hyperintensity. (For interpretation of the references to color in this figure legend, the reader is referred to the Web version of this article.)

using MCFLIRT in FMRIB Software Library (FSL) (Alsop et al., 2015; Jenkinson et al., 2002). The M0 image was not acquired during the scan session. Therefore, M0 image was calculated using the first control image, knowing the timing of the BS pulses and excitation pulses, the M0 image was calculated from the first control image using Bloch equations. The equation for M0 calculation was

$$M_z = M_0 \left(1 - 2e^{-\frac{\Delta BS2}{T1}} + 2e^{-\frac{-(\Delta BS1 + \Delta BS2)}{T1}} + 2e^{-\frac{-(BS2 + \Delta BS2)}{T1}} \right), \quad (1)$$

where M_z is the magnetization from the first control image, BS1 and BS2 are the timings of the background suppression pulses after the labeling pulses, $\Delta BS1$ is the duration between the 2 BS pulses, and $\Delta BS2$ is the duration between the second BS pulse and the excitation pulse. Note that this equation neglects the effect of the saturation pulses applied before labeling begins. The T1 was chosen appropriately based on whether the tissue was predominantly GM (T1 = 1331 ms), WM (T1 = 832 ms), or cerebrospinal fluid (T1 = 4100 ms) (Chen et al., 2001; Wansapura et al., 1999). Tissue classification was done based on T1 segmentation using FSL FAST (Zhang et al., 2001).

Similar calculations were performed in other studies (Donahue et al., 2006). The purpose of calculating the M0 was to quantify absolute CBF instead of using relative perfusion weighted values. To ensure that this approach did not alter interpretations, we implemented the same sequence with and without M0 acquisition in 9 young healthy subjects (post hoc). We then compared the CBF measurements using a true M0 image and a calculated M0 image and ensured that CBF values were tightly correlated within each subject (average correlation across subjects, $r = 0.92 \pm 0.03$, Supplementary Figure 1 for overall cortical CBF. CBF values with the estimated M0 map were only slightly lower than those estimated with an acquired M0 map by a factor of 0.97 ± 0.06). CBF values were measured and compared in the frontal, temporal, parietal, and occipital lobes as well as in the caudate, putamen, thalamus, hippocampus, amygdala, normal-appearing WM, and WMHs. All regional CBF values were adjusted for GM density to account for CBF reductions due to partial

volume effects with WM and cerebrospinal fluid. All comparisons were performed using paired *t*-tests.

For CVR quantification, the breath-hold time course was first subsampled to match the TR of the BOLD acquisitions. The subsampled time course was then convolved with the respiratory response function (Birn et al., 2008). This function has been shown to better reflect the cerebral vascular response than the conventional hemodynamic response function and accounts for the circulation delay in the cerebrovascular response due to breathing. The new convolved time course was then used as a stimulus time course for FSL FEAT (FSL v5.0, Woolrich et al., 2009). In FEAT, we performed motion correction using MCFLIRT, brain extraction, baseline drift correction, and smoothing (full-width-half maximum (FWHM) = 5 mm). Standard GM and WM masks from FSL in Montreal Neurological Institute (MNI) space (2 mm) were applied to the FEAT output using FEAT query to obtain percent signal change in the 2 tissue types. We ensured that the amplitude of the time course fluctuated between 0 and 1 for correct interpretation of the FEAT query results.

For the WMHs, the Flex automatic lesion detection algorithm was applied to the FLAIR images, and binary masks of the hyperintensities were obtained (Gibson et al., 2010). The number of voxels and subsequently volume of the binary masks were calculated and divided by the total intracranial volume to obtain the percent of brain occupied by the WMHs, that is, hyperintensity burden. The total intracranial volume was calculated using FreeSurfer v5.3 (estimated total intracranial volume (eTIV); Dale et al., 1999). WMH burden represented the total burden due to both perivascular and deep WMHs. Normal-appearing WM was all brain WM excluding the hyperintense voxels considered as lesions and identified using the FLAIR image.

The standard space MNI atlas was resampled to 3-mm space. The FLAIR images were then downsampled to an isotropic resolution of 3 mm³. The CBF and CVR images were then subsequently registered and resampled to match the 3-mm MNI space and the corresponding FLAIR images.

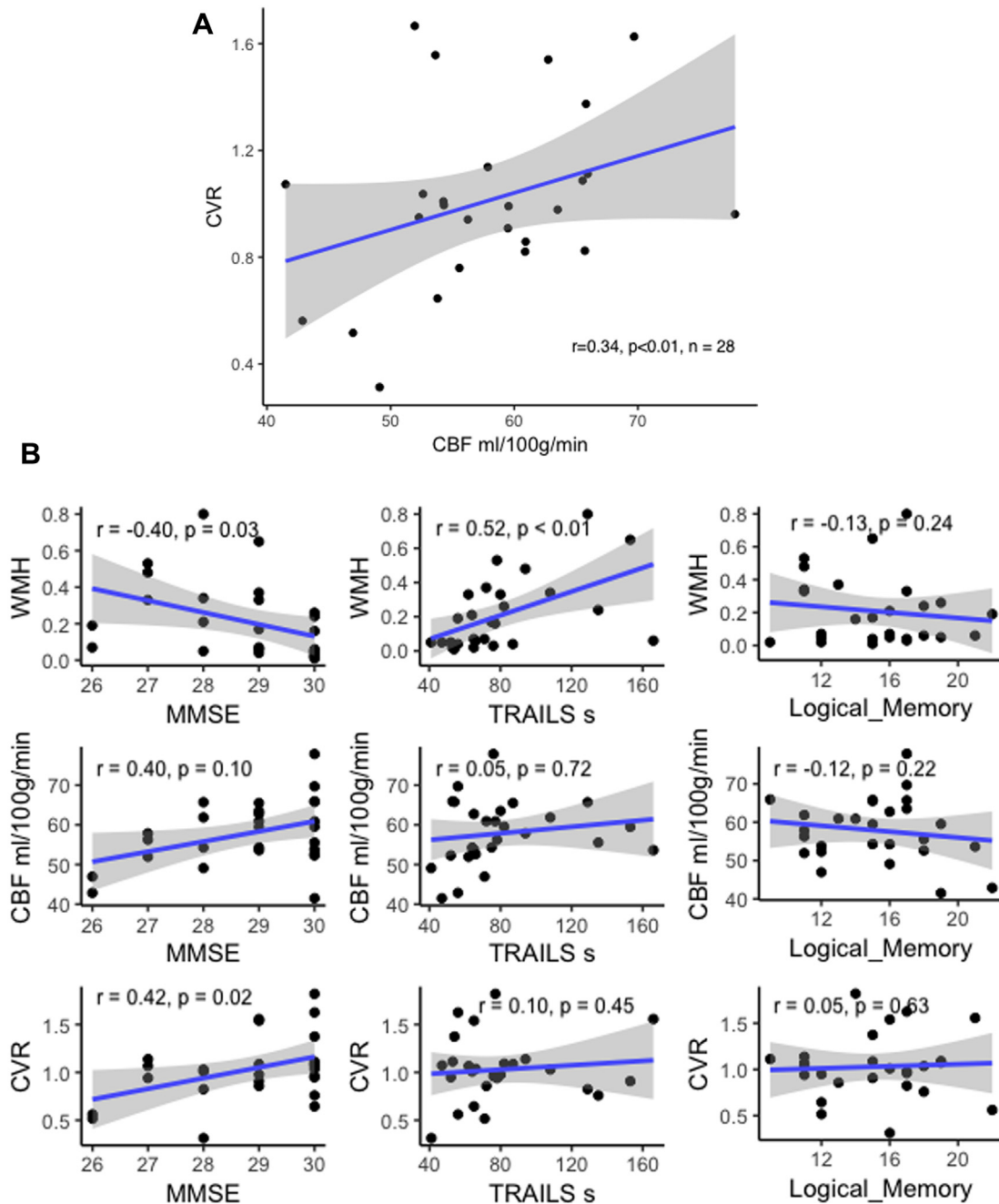


Fig. 2. Overall cortical CBF and CVR values are directly proportional to cognitive status of subjects. Subjects with low CBF and low CVR had poor MMSE scores. Note that although the correlation between CBF and CVR is statistically significant (A), only 12.25% (R^2) of the variance in the data is explained by this relationship. (B) High WMH burden (number of voxels with WMHs divided by total intracranial volume) was a strong indicator of poor performance on MMSE and Trails. High CVR was related to high MMSE scores (significant) and quicker processing times on Trails (marginally significant). Relationship between CBF and cognitive performance was the weakest of the 3 vascular pathology markers in healthy older adults. Logical memory did not appear to be correlated with any marker. r = Pearson's correlation, p significance of association between cognitive test and vascular marker after adjusting for age and diagnosis. Abbreviations: CBF, cerebral blood flow; CVR, cerebrovascular reserve; MMSE, Mini-Mental State Examination; WMH, white matter hyperintensity.

The WMH mask was then dilated by 1 voxel (3 mm) in all directions to obtain the penumbra of tissue surrounding the hyperintensity that is likely at risk of tissue infarction. This dilation process was repeated 5 times to assess the spatial changes in CBF and CVR in the tissue surrounding the WMHs. Percent decrease in CBF and CVR were calculated using the outermost layer of tissue as baseline (15 mm from the hyperintensity) with 5 spatial points. Curve fitting was performed in MATLAB R2016b to determine the relationship between percent decrease in CBF or CVR and distance

from the WMH. CBF and CVR values within the WMHs and 3, 6, 9, 12, and 15 mm away from the hyperintensities were measured and compared using a paired t -test.

Correlation of GM CBF and CVR as well as WMH burden (normalized by total intracranial volume), with MMSE as a measure of overall cognitive function, was evaluated. Since WMH burden is strongly associated with task processing speed, we also evaluated the association of CBF and CVR with performance on the Trails, part B, as a measure of executive function.

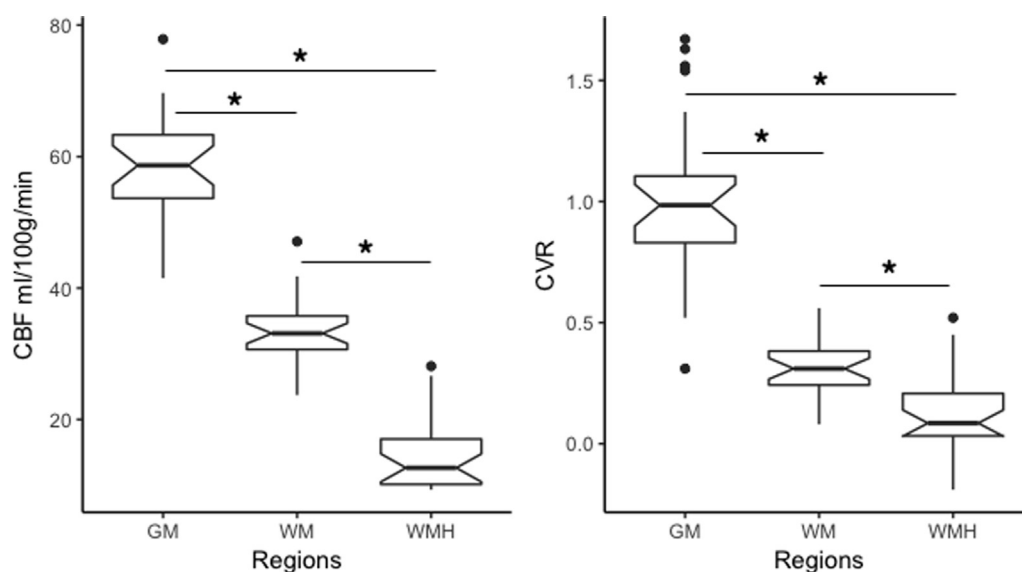


Fig. 3. Plots (A) and (B) show CBF and CVR, respectively, in the GM, WM, and WMHs. WM includes all-brain WM but not the WMHs. CBF is significantly different between GM and WM, as well as between the WM and WMHs. CVR also is significantly different between GM, WM, and WMHs. (* $p < 0.05$). Black circles indicates outliers as in any typical whisker plot. Abbreviations: CBF, cerebral blood flow; CVR, cerebrovascular reserve; GM, gray matter; WM, white matter; WMH, white matter hyperintensity.

3. Results

Of the 28 individuals, 7 subjects were identified with mild cognitive impairment based on consensus diagnosis as outlined previously. For the following results, all subjects were considered as a single group except while evaluating the association between cognitive performance, CBF, CVR, and hyperintensity burden. For these tests, the associations were adjusted for age and cognitive status.

3.1. Multimodal vascular imaging markers

Fig. 1 shows group-level (A) and single-subject (B) maps for CVR (top row), CBF (middle row), and WMHs (bottom row). The bottom row shows the regional distribution of WMHs across all subjects in the group level. Red indicates higher frequency of finding WMHs, whereas blue indicates a lower frequency of WMHs. In Fig. 1B, the green mask represents WMHs segmentation in a single subject. The CVR maps show higher BOLD signal intensity change across all GM representing a vasodilatory response following a breath-hold stimulus. In the single-subject map, a negative BOLD response is also observed near the location of the WMHs. The negative response is likely due to steal phenomenon (Mandell et al., 2008; Poubanc et al., 2013), that is, diversion of blood flow from vasculature perfusing the WMHs to surrounding brain regions with healthy tissue structure, or due to the compression of cerebrospinal fluid in the ventricular compartment, also in the vicinity of the WMHs. The average GM CBF was 57.9 ± 8.1 mL/100 g/min and GM CVR was $1.0 \pm 0.03\%$. Average WM burden (including both periventricular and deep WM) was $0.21 \pm 0.21\%$ of the total intracranial volume.

3.2. Correlation of vascular markers with cognitive performance

CBF and CVR were significantly correlated with each other (Fig. 2A, $r = 0.34$, $p < 0.05$, $n = 28$). Linear regression model, after adjusting for age and diagnosis, showed a trend toward correlation between MMSE and CBF ($p = 0.1$; Pearson's correlation between CBF and MMSE, $r = 0.40$), and a significant correlation between MMSE and CVR ($p = 0.02$; $r = 0.42$). The p -values reflect the regression output showing association of CBF and CVR with MMSE

after accounting for the effect of age and diagnosis. After adjusting for age and diagnosis, Trails B scores were not related significantly with CBF ($p = 0.72$; $r = 0.05$) or CVR ($p = 0.45$; $r = 0.10$). High WMH burden was associated with poorer MMSE scores and with longer processing times on the Trails B test (Fig. 2B, $p = 0.03$; $r = -0.40$ for MMSE and 0.006 ; $r = 0.52$ for Trails B). No correlation was observed with logical memory scores for CBF ($p = 0.22$; $r = -0.12$), CVR ($p = 0.63$; $r = 0.05$), or WMHs ($p = 0.24$; $r = -0.13$).

In addition, although not significant, the apolipoprotein E (APOE)- $\epsilon 4$ carriers had lower CBF ($n = 5$, 57.5 ± 4.23 mL/100 g/min), CVR (0.99 ± 0.08), and higher WMH burden (0.33 ± 0.19) compared to the noncarriers (CBF: $n = 23$, 57.9 ± 9.07 mL/100 g/min; CVR: 1.00 ± 0.37 ; and hyperintensity burden: 0.17 ± 0.21). Of the 5 APOE- $\epsilon 4$ carriers, 4 were cognitively normal older adults and 1 individual had mild cognitive impairment.

3.3. Regional variations in CBF and CVR

Fig. 3 depicts regional CBF and CVR values in all GM as well as WM and WMHs. Table 2 lists the CBF and CVR in the different

Table 2
Regional variations in CBF and CVR in older adults

Region	CBF (mL/100 g/min)		CVR (% signal)	
	Mean	Standard deviation	Mean	Standard deviation
Frontal cortex	57.2	8.3	1.00	0.40
Temporal cortex	63.1	9.0	0.94	0.32
Parietal cortex	65.8	9.6	1.18	0.42
Occipital cortex	42.2	16.3	1.35	0.54
Insula	55.4	6.7	0.61	0.25
Caudate	52.9	18.2	0.55	0.32
Putamen	45.7	9.1	1.50	0.84
Thalamus	39.2	12.7	2.41	0.91
Hippocampus	41.7	8.6	0.87	0.48
Amygdala	70.1	25.9	0.98	0.57
Total gray matter	57.9	8.1	1.00	0.03
Total white matter	33.1	5.3	0.32	0.11
White matter hyperintensities ^a	16.9	5.9	0.12	0.15

Key: CBF, cerebral blood flow; CVR, cerebrovascular reserve.

^a Includes both periventricular and deep white matter hyperintensities.

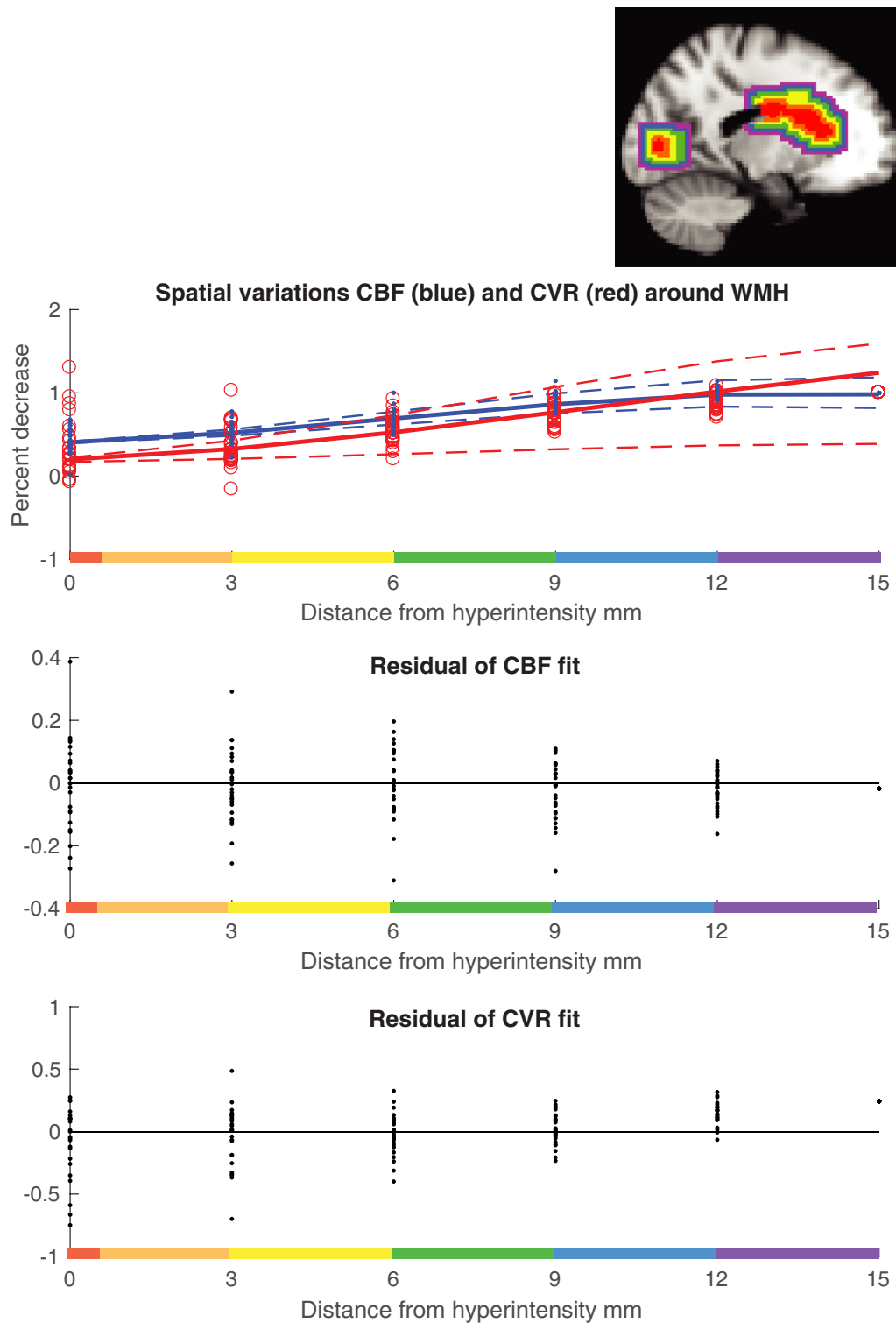


Fig. 4. Top row indicates CBF (closed blue circles) and CVR (open red circles) changes within the WMH (0 mm = red) and 3 (orange), 6 (yellow), 9 (green), 12 (blue), and 15 (purple) mm away from the hyperintensity as shown in the inset image. Both CBF and CVR decrease as we approach the WMH. CVR decreases ($79.3 \pm 48.9\%$) are significantly higher than CBF decreases ($58.4 \pm 13.9\%$). Bottom 2 rows indicate residual for the nonlinear fits of CBF and CVR, respectively. Abbreviations: CBF, cerebral blood flow; CVR, cerebrovascular reserve; WMH, white matter hyperintensity. (For interpretation of the references to color in this figure legend, the reader is referred to the Web version of this article.)

brain regions. No significant difference was observed between the CBF values in the different GM regions. CBF in the WM and WMHs was significantly different from all GM regions. CBF and CVR in the WMHs were both significantly lower than all other

brain regions. CBF and CVR in the WM were also significantly ($p < 0.05$) lower than that in the GM regions.

The size of WMHs was inversely proportional to the GM CBF ($n = 28$, $r = -0.10$, not significant) and CVR ($n = 28$, $r = -0.16$, not significant).

3.4. Spatial patterns of CBF and CVR in and around WMHs

Fig. 4 shows how CBF and CVR vary in the tissue surrounding the WMHs. Average CBF value within the hyperintensities was 13.9 ± 5.9 mL/100 g/min. CBF values were 17.6 ± 5.2 , 22.8 ± 5.59 , 29.5 ± 5.3 , 33.0 ± 4.9 , and 33.1 ± 5.0 mL/100 g/min at 3, 6, 9, 12, and 15 mm, respectively, from the hyperintensity. Average CVR value within the hyperintensities was $0.12 \pm 0.15\%$. CVR values were 0.16 ± 0.10 , 0.23 ± 0.10 , 0.32 ± 0.11 , 0.38 ± 0.13 , and $0.43 \pm 0.14\%$ at 3, 6, 9, 12, and 15 mm, respectively, from the hyperintensity and significantly different ($p < 0.005$) from CVR in the hyperintensity. CBF values between 0, 3, 6, and 9 mm distance from the WMHs were significantly different from each other. CBF values in the WMHs decreased by $58.4 \pm 13.9\%$ compared to that at 15 mm. There was no difference between CBF values at 9 and 12 mm from the WMHs. However, CVR values were significantly different at 0, 3, 6, and 9 as well as 12 mm distance from the WMHs. CVR values in the WMHs decreased by $79.3 \pm 48.9\%$ (significantly greater than CBF decreases, $p < 0.05$) compared to that at 15 mm.

Percent decrease in CBF was nonlinearly proportional to the distance from the WMH, that is, closer the tissue voxel to the hyperintensity, greater the decrease in CBF ($R^2 = 0.98$, adjusted $R^2 = 0.98$ for a cubic fit). Percent decrease in CVR was also nonlinearly proportional to the distance from the WMH ($R^2 = 0.95$, adjusted $R^2 = 0.95$ for a cubic fit). Residual plots for both fits are shown below. We, therefore, conclude that CVR is a more sensitive measure of cerebrovascular morbidity compared to CBF.

4. Discussion

In this work, we show that (1) compared to CBF, CVR is a more sensitive measure of compromised vasculature and (2) both CBF and CVR correlate with MMSE status. Only CVR was correlated with Trails B. WMH burden was correlated with MMSE as well as processing speed in Trails B. Based on our finding, we believe that CVR can be an early marker of tissue ischemia and can be applied to evaluate risk of developing WMHs.

4.1. CBF and CVR as imaging markers of vascular pathology in small vessel disease

In Fig. 4, we show that CVR decreases much more rapidly than CBF. Although CBF and CVR are strongly positively correlated, CVR decreases in the tissue surrounding the WMHs are larger than the corresponding CBF decreases. This is an important finding. CBF reductions are in part due to neurodegeneration and likely also due to loss of vascular reserve. This is in accordance with recent studies showing slower reductions in CBF in AD compared to reductions in CVR (Gao et al., 2013; Liu et al., 2014). It is therefore likely that CVR is an earlier predictor of vascular failure and tissue infarction compared to CBF.

4.2. Paradigm selection for CVR measurement

In this study, we used a breath-hold paradigm for CVR calculations. Several issues need to be discussed. There are multiple ways to measure CVR. BOLD is a semiquantitative approach compared to ASL-derived CVR (Donahue et al., 2014; Faraco et al., 2015). Because BOLD signal has a significantly higher signal-to-noise ratio and has greater temporal resolution than ASL, we believe that BOLD signal response is more sensitive than the ASL signal for a breath-hold challenge. The change in EtCO₂ in a breath-hold task was found to be approximately 3 mm Hg compared to typical hypercapnic gas challenges, where the change in EtCO₂ is about 15 mm Hg in young adults (<40 years of age; Murphy et al., 2011). It is likely that this EtCO₂ change is even smaller in magnitude in older adults. Our

cortical GM CVR was $1.00 \pm 0.03\%$ for 15 seconds breath-hold. This result is similar to the CVR obtained by other studies using a paced breath-hold paradigm (<1% in Chang and Glover, 2009; and 0.43% for 9 seconds breath-hold in Magon et al., 2009). Although the magnitude of CVR response with a hypercapnic gas challenge is an order of magnitude higher (2%–5%) than the breath-hold challenge, our preference for breath-hold was due to the ease of implementation. No additional equipment was needed. We believe that the absence of the breathing apparatus increases subject co-operation. The drawback is that the study relies heavily on accurate placement of the respiratory bellows. The subjects in this study were trained outside the scanner to perform the breath-hold paradigm until they are able to follow the written instructions well.

4.3. Perfusion measurements using ASL

CBF measurements using ASL is now a routine measurement that is readily available in the clinic. We used this method to measure perfusion in older adults and found correlation between cortical CBF and MMSE scores. This correlation between regional perfusion and cognitive tests has been observed in many other studies. It is likely that reduced CBF can serve as a functional MRI marker of cerebrovascular disease and poor cognitive performance. We also show some regional variations in CBF; however, they were not significant. Note that most studies use a label duration around 1500 ms and a post-labeling delay of 1650 ms, which is insufficient to accurately quantify WM CBF and is likely unsuitable for quantitative comparison across groups (van Osch et al., 2009). However, ASL signal in the WMHs and WM will still be proportional to tissue perfusion and hence can provide information regarding slowed perfusion in abnormal tissue compared to normal tissues within a subject and as shown in all previous studies of perfusion in WMHs (Brickman et al., 2009; van Dalen et al., 2016; Promjunyakul et al., 2015).

4.4. Location of WMHs

We calculated total WMH burden without separating periventricular and deep WM contributions. Our current analyses did not support the separation of the hyperintensities based on location. The pathologic origins of the 2 hyperintensities are believed to be distinct; periventricular hyperintensities occur due to venous collagenosis, whereas deep WMHs due to arterial insufficiency (Pantoni and Garcia, 1997). It is likely that the reduced CBF and CVR may be more strongly associated with deep WMHs. Future work will involve separating the WMHs based on location and evaluating correlations with CBF, CVR, and cognitive performance.

5. Conclusion

We show feasibility of ASL and breath-hold BOLD to evaluate CBF and CVR as markers of cerebrovascular disease in older adults. Although both CBF and CVR are indicators of declining cognitive performance in this cohort, our study showed that CVR is a more sensitive marker of tissue infarction and cerebrovascular disease compared to CBF. Future studies will investigate whether reduced CVR around the WMHs can be measured longitudinally to predict tissue voxels at risk of infarction.

Disclosure statement

The authors report no conflicts of interest.

Acknowledgements

Authors' contributions: SR and NK are responsible for processing and analyses of data and manuscript preparation. MKA and PB are responsible for experimental setup and data acquisition, and TM assisted with software tools for data analysis. TJG, BC, SJ, and EL coordinated the MRI and subject recruitment as well as supervised the manuscript preparation.

This research did not receive any specific grant from funding agencies in the public, commercial, or not-for-profit sectors. Institutional funds were provided by University of Washington School of Medicine to TJG. Analysis effort by SR was partly supported by K01AG055669 (NIH/NIA).

Appendix A. Supplementary data

Supplementary data associated with this article can be found, in the online version, at <https://doi.org/10.1016/j.neurobiolaging.2018.01.006>.

References

- Al-Bachari, S., Parkes, L.M., Vidyasagar, R., Hanby, M.F., Tharaken, V., Leroi, I., Emsley, H.C., 2014. Arterial spin labelling reveals prolonged arterial arrival time in idiopathic Parkinson's disease. *Neuroimage* 6, 1–8.
- Alsop, D.C., Detre, J.A., Golay, X., Günther, M., Hendrikse, J., Hernandez-Garcia, L., Lu, H., MacIntosh, B.J., Parkes, L.M., Smits, M., Osch, M.J., 2015. Recommended implementation of arterial spin-labeled perfusion MRI for clinical applications: a consensus of the ISMRM perfusion study group and the European consortium for ASL in dementia. *Magn. Reson. Med.* 73, 102–116.
- Au, R., Massaro, J.M., Wolf, P.A., Young, M.E., Beiser, A., Seshadri, S., D'Agostino, R.B., DeCarli, C., 2006. Association of white matter hyperintensity volume with decreased cognitive functioning: the Framingham Heart Study. *Arch. Neurol.* 63, 246–250.
- Bahrani, A.A., Powell, D.K., Yu, G., Johnson, E.S., Jicha, G.A., Smith, C.D., 2017. White matter hyperintensity associations with cerebral blood flow in elderly subjects stratified by cerebrovascular risk. *J. Stroke Cerebrovasc. Dis.* 26, 779–786 (available online).
- Beekly, D.L., Ramos, E.M., Lee, W.W., Deitrich, W.D., Jacka, M.E., Wu, J., Hubbard, J.L., Koepsell, T.D., Morris, J.C., Kukull, W.A., 2007. The National Alzheimer's Coordinating Center (NACC) database: the uniform data set. *Alzheimer Dis. Assoc. Disord.* 21, 249–258.
- Birn, R.M., Smith, M.A., Jones, T.B., Bandettini, P.A., 2008. The respiration response function: the temporal dynamics of fMRI signal fluctuations related to changes in respiration. *Neuroimage* 40, 644–654.
- Bots, M.L., Hoes, A.W., Koudstaal, P.J., Hofman, A., Grobbee, D.E., 1997. Common carotid intima-media thickness and risk of stroke and myocardial infarction the Rotterdam Study. *Circulation* 96, 1432–1437.
- Brickman, A.M., Zahra, A., Muraskin, J., Steffener, J., Holland, C.M., Habeck, C., Borogovac, A., Ramos, M.A., Brown, T.R., Asllani, I., Stern, Y., 2009. Reduction in cerebral blood flow in areas appearing as white matter hyperintensities on magnetic resonance imaging. *Psychiatry Res.* 172, 117–120.
- Bright, M.G., Murphy, K., 2013. Reliable quantification of BOLD fMRI cerebrovascular reactivity despite poor breath-hold performance. *Neuroimage* 83, 559–568.
- Chang, C., Glover, G.H., 2009. Relationship between respiration, end-tidal CO₂, and BOLD signals in resting-state fMRI. *Neuroimage* 47, 1381–1393.
- Chen L, Bernstein M, Huston J, Fain S, 2001. Measurements of T1 relaxation times at 3.0 T: implications for clinical MRA. In Proceedings of the 9th Annual Meeting of ISMRM, Glasgow, Scotland.
- Dale, A.M., Fischl, B., Sereno, M.I., 1999. Cortical surface-based analysis: I. Segmentation and surface reconstruction. *Neuroimage* 9, 179–194.
- de Groot, J.C., Oudkerk, M., Gijn, J.V., Hofman, A., Jolles, J., Breteler, M.M., 2000. Cerebral white matter lesions and cognitive function: the Rotterdam Scan Study. *Ann. Neurol.* 47, 145–151.
- Detre, J.A., Zhang, W., Roberts, D.A., Silva, A.C., Williams, D.S., Grandis, D.J., Kortessy, A.P., Leigh, J.S., 1994. Tissue specific perfusion imaging using arterial spin labeling. *NMR Biomed.* 7, 75–82.
- Donahue, M.J., Faraco, C.C., Strother, M.K., Chappell, M.A., Rane, S., Dethrage, L.M., Hendrikse, J., Siero, J.C., 2014. Bolus arrival time and cerebral blood flow responses to hypercarbia. *J. Cereb. Blood Flow Metab.* 34, 1243–1252.
- Dufouil, C., Chalmers, J., Coskun, O., Besancon, V., Boussier, M.G., Guillon, P., Macmahon, S., Mazoyer, B., Neal, B., Woodward, M., Tzourio-Mazoyer, N., 2005. Effects of blood pressure lowering on cerebral white matter hyperintensities in patients with stroke. *Circulation* 112, 1644–1650.
- Donahue, M.J., Lu, H., Jones, C.K., Edden, R.A., Pekar, J.J., van Zijl, P., 2006. Theoretical and experimental investigation of the VASO contrast mechanism. *Magn. Reson. Med.* 56, 1261–1273.
- Esiri, M.M., Nagy, Z., Smith, M.Z., Barnetson, L., Smith, A.D., 1999. Cerebrovascular disease and threshold for dementia in the early stages of Alzheimer's disease. *Lancet* 354, 919–920.
- Faraco, C.C., Strother, M.K., Dethrage, L.M., Jordan, L., Singer, R., Clemmons, P.F., Donahue, M.J., 2015. Dual echo vessel-encoded ASL for simultaneous BOLD and CBF reactivity assessment in patients with ischemic cerebrovascular disease. *Magn. Reson. Med.* 73, 1579–1592.
- Farkas, E., Luiten, P.G., 2001. Cerebral microvascular pathology in aging and Alzheimer's disease. *Prog. Neurobiol.* 64, 575–611.
- Folstein, M.F., Folstein, S.E., McHugh, P.R., 1975. "Mini-mental state": a practical method for grading the cognitive state of patients for the clinician. *J. Psychiatr. Res.* 12, 189–198.
- Gao, Y.Z., Zhang, J.J., Liu, H., Wu, G.Y., Xiong, L., Shu, M., 2013. Regional cerebral blood flow and cerebrovascular reactivity in Alzheimer's disease and vascular dementia assessed by arterial spin labeling magnetic resonance imaging. *Curr. Neurovasc. Res.* 10, 49–53.
- Gibson, E., Gao, F., Black, S.E., Lobaugh, N.J., 2010. Automatic segmentation of white matter hyperintensities in the elderly using FLAIR images at 3T. *J. Magn. Reson. Imaging* 31, 1311–1322.
- Gückel, F.J., Brix, G., Schmiedek, P., Piepgras, Z., Becker, G., Köpke, J., Gross, H., Georgi, M., 1996. Cerebrovascular reserve capacity in patients with occlusive cerebrovascular disease: assessment with dynamic susceptibility contrast-enhanced MR imaging and the acetazolamide stimulation test. *Radiology* 201, 405–412.
- Jenkinson, M., Bannister, P., Brady, M., Smith, S., 2002. Improved optimization for the robust and accurate linear registration and motion correction of brain images. *Neuroimage* 17, 825–841.
- Kastrup, A., Li, T.Q., Takahashi, A., Glover, G.H., Moseley, M.E., 1998. Functional magnetic resonance imaging of regional cerebral blood oxygenation changes during breath holding. *Stroke* 29, 2641–2645.
- Liao, D., Cooper, L., Cai, J., Toole, J.F., Bryan, N.R., Hutchinson, R.G., Tyroler, H.A., 1996. Presence and severity of cerebral white matter lesions and hypertension, its treatment, and its control. *Stroke* 27, 2262–2270.
- Liem, M.K., Oberstein, S.L., Haan, J., Boom, R., Ferrari, M.D., Buchem, M., Grond, J., 2009. Cerebrovascular reactivity is a main determinant of white matter hyperintensity progression in CADASIL. *Am. J. Neuroradiol.* 30, 1244–1247.
- Liu, P., Lu, H., Rodrigue, K., Kennedy, K., Peng, S.L., Devous, M.D., Park, D.C., 2014. Impact of beta-amyloid burden on brain perfusion and vascular reactivity in normal aging. *Alzheimers Dement.* 10, P143–P144.
- Mack, W.J., Freed, D.M., Williams, B.W., Henderson, V.W., 1992. Boston Naming Test: shortened versions for use in Alzheimer's disease. *J. Gerontol.* 47, P154–P158.
- Magon, S., Basso, G., Faraco, P., Ricciardi, G.K., Beltramello, A., Sbarbati, A., 2009. Reproducibility of BOLD signal change induced by breath holding. *Neuroimage* 45, 702–712.
- Makedonov, I., Black, S.E., MacIntosh, B.J., 2013. Cerebral small vessel disease in aging and Alzheimer's disease: a comparative study using MRI and SPECT. *Eur. J. Neurol.* 20, 243–250.
- Mandell, D.M., Han, J.S., Poubanc, J., Crawley, A.P., Kassner, A., Fisher, J.A., Mikulis, D.J., 2008. Selective reduction of blood flow to white matter during hypercapnia corresponds with leukoaraiosis. *Stroke* 39, 1993–1998.
- Marstrand, J.R., Garde, E., Rostrop, E., Ring, P., Rosenbaum, S., Mortensen, E.L., Larsson, H.B., 2002. Cerebral perfusion and cerebrovascular reactivity are reduced in white matter hyperintensities. *Stroke* 33, 972–976.
- Molina, C., Sabin, J.A., Montaner, J., Rovira, A., Abilleira, S., Codina, A., 1999. Impaired cerebrovascular reactivity as a risk marker for first-ever lacunar infarction. *Stroke* 30, 2296–2301.
- Montine, T., Sonnen, J.A., Montine, K.S., Crane, P.K., Larson, E.B., 2012. Adult changes in thought study: dementia is an individually varying convergent syndrome with prevalent clinically silent diseases that may be modified by some commonly used therapeutics. *Curr. Alzheimer Res.* 9, 718–723.
- Murphy, K., Harris, A.D., Wise, R.G., 2011. Robustly measuring vascular reactivity differences with breath-hold: normalising stimulus-evoked and resting state BOLD fMRI data. *Neuroimage* 54, 369–379.
- Novak, V., Last, D., Alsop, D.C., Abduljalil, A.M., Hu, K., Lepicovsky, L., Cavallerano, J., Lipsitz, L.A., 2006. Cerebral blood flow velocity and periventricular white matter hyperintensities in type 2 diabetes. *Diabetes care* 29, 1529–1534.
- Pantoni, L., 2010. Cerebral small vessel disease: from pathogenesis and clinical characteristics to therapeutic challenges. *Lancet Neurol.* 9, 689–701.
- Pantoni, L., Garcia, J.H., 1997. Pathogenesis of leukoaraiosis. *Stroke* 28, 652–659.
- Poubanc, J., Han, J.S., Mandell, D.M., Conklin, J., Stainsby, J.A., Fisher, J.A., Mikulis, D.J., Crawley, A.P., 2013. Vascular steal explains early paradoxical blood oxygen level-dependent cerebrovascular response in brain regions with delayed arterial transit times. *Cerebrovasc. Dis. Extra* 3, 55–64.
- Prins, N.D., Scheltens, P., 2015. White matter hyperintensities, cognitive impairment and dementia: an update. *Nat. Rev. Neurol.* 11, 157–165.
- Promjunyakul, N., Lahna, D., Kaye, J.A., Dodge, H.H., Erten-Lyons, D., Rooney, W.D., Silbert, L.C., 2015. Characterizing the white matter hyperintensity penumbra with cerebral blood flow measures. *Neuroimage* 8, 224–229.
- Sam, K., Crawley, A.P., Conklin, J., Poubanc, J., Sobczyk, O., Mandell, D.M., Venkatraghavan, L., Duffin, J., Fisher, J.A., Black, S.E., Mikulis, D.J., 2016. Development of white matter hyperintensity is preceded by reduced cerebrovascular reactivity. *Ann. Neurol.* 80, 277–285.
- Smith, E.E., Salat, D.H., Jeng, J., McCreary, C.R., Fischl, B., Schmahmann, J.D., Dickerson, B.C., Viswanathan, A., Albert, M.S., Blacker, D., Greenberg, S.M., 2011. Correlations between MRI white matter lesion location and executive function and episodic memory. *Neurology* 76, 1492–1499.

- Tombaugh, T.N., 2004. Trail Making Test A and B: normative data stratified by age and education. *Arch. Clin. Neuropsychol.* 19, 203–214.
- van Dalen, J.W., Mutsaerts, H.J., Nederveen, A.J., Vrenken, H., Steenwijk, M.D., Caan, M.W., Majoie, C.B., van Gool, W.A., Richard, E., 2016. White matter hyperintensity volume and cerebral perfusion in older individuals with hypertension using arterial spin-labeling. *Am. J. Neuroradiol.* 37, 1824–1830.
- van Osch, M.J., Teeuwisse, W.M., van Walderveen, M.A., Hendrikse, J., Kies, D.A., van Buchem, M.A., 2009. Can arterial spin labeling detect white matter perfusion signal? *Magn. Reson. Med.* 62, 165–173.
- Wansapura, J.P., Holland, S.K., Dunn, R.S., Ball, W.S., 1999. NMR relaxation times in the human brain at 3.0 tesla. *J. Magn. Reson. Imaging* 9, 531–538.
- Wardlaw, J.M., Smith, E.E., Biessels, G.J., Cordonnier, C., Fazekas, F., Frayne, R., Lindley, R.L., O'Brien, J.T., Barkhof, F., Benavente, O.R., Black, S.E., 2013. Neuroimaging standards for research into small vessel disease and its contribution to ageing and neurodegeneration. *Lancet Neurol.* 12, 822–838.
- Wechsler, D., 1945. A standardized memory scale for clinical use. *J. Psychol.* 19, 87–95.
- Wechsler, D., 2014. Wechsler Adult Intelligence Scale—Fourth Edition (WAIS–IV), San Antonio, Texas, Psychological Corporation.
- White, L., Petrovitch, H., Ross, G.W., Masaki, K.H., Abbott, R.D., Teng, E.L., Rodriguez, B.L., Blanchette, P.L., Havlik, R.J., Wergowske, G., Chiu, D., 1996. Prevalence of dementia in older Japanese-American men in Hawaii: the Honolulu-Asia aging study. *JAMA* 276, 955–960.
- Wong, E.C., Buxton, R.B., Frank, L.R., 1999. Quantitative perfusion imaging using arterial spin labeling. *Neuroimaging Clin.* 9, 333–342.
- Woolrich, M.W., Jbabdi, S., Patenaude, B., Chappell, M., Makni, S., Behrens, T., Beckmann, C., Jenkinson, M., Smith, S.M., 2009. Bayesian analysis of neuroimaging data in FSL. *Neuroimage* 45, S173–S186.
- Zhang, Y., Brady, M., Smith, S., 2001. Segmentation of brain MR images through a hidden Markov random field model and the expectation-maximization algorithm. *IEEE Trans. Med. Imaging* 20, 45–57.